Electronic structure of the photoactive yellow protein chromophore: Ab initio study of the low-lying excited singlet states

ARTICLE *in* JOURNAL OF PHOTOCHEMISTRY AND PHOTOBIOLOGY A CHEMISTRY · AUGUST 2007

Impact Factor: 2.5 · DOI: 10.1016/j.jphotochem.2007.04.033

Available online at www.sciencedirect.com
ScienceDirect
Journal of Photochemistry and Photobiology A: Chemistry 190 (2007) 241–257
Journal of Photochemistry and Photobiology A:Chemistry
www.elsevier.com/locate/jphotochem

Electronic structure of the photoactive yellow protein chromophore: Ab initio study of the low-lying excited singlet states

Evgeniy V. Gromov [a,b], Irene Burghardt [c,*], James T. Hynes [c,d], Horst Köppel [a], Lorenz S. Cederbaum [a]

[a] *Theoretische Chemie, Physikalisch-Chemisches Institut Universität Heidelberg, Im Neuenheimer Feld 229, D-69120 Heidelberg, Germany*
[b] *Laboratory of Quantum Chemistry, Computer Center, Irkutsk State University, K. Marks 1, 664003 Irkutsk, Russian Federation*
[c] *Département de Chimie, Ecole Normale Supérieure, 24 rue Lhomond, F-75231 Paris Cedex 05, France*
[d] *Department of Chemistry and Biochemistry, University of Colorado, Boulder, CO 80309-0215, USA*

Received 14 March 2007; received in revised form 30 April 2007; accepted 30 April 2007
Available online 5 May 2007

Abstract

The excited electronic states of the *p*-coumaric acid thio-ester chromophore of the Photoactive Yellow Protein (PYP) are characterized in view of identifying the key factors determining the chromophore's isomerisation. These factors include the anionic nature of the chromophore, the presence of sulfur (rather than oxygen or nitrogen) in the ester moiety, and the presence of a hydrogen-bonding environment stabilizing the phenolate moiety. Two twisted stationary S_1 structures are identified, corresponding to a twist around the double bond conjugated with the aromatic ring, and the single bond adjacent to the ring, respectively. The latter structure is accessed directly by relaxation from the Franck–Condon (FC) geometry. These structures are shown to entail a substantial polarization effect (increasing charge separation when moving towards the twisted geometry). Further, an inversion of charge character is observed for the double-bond twisted minimum, which can be accounted for by the vicinity of an S_1–S_0 conical intersection. The S_1–S_0 gap at the minimum geometries depends in a sensitive fashion on the α-carbonyl heteroatom. Based upon these observations for the intrinsic properties of the chromophore, we further address the effect of the Arg52 residue, which acts as a counter-ion in the native protein environment.

Keywords: PYP; PYP chromophore; Excited states; *cis–trans* isomerisation; CC2 method; EOM-CCSD method; Conical intersection; Polarization; Effects of the protein environment

1. Introduction

The excited-state electronic structure of coumaric acid and its sulfur containing analogs has recently attracted much attention, in view of characterizing the *p*-coumaric thio-ester chromophore of the photoactive yellow protein (PYP). PYP is a photoreceptor protein occurring in the *Halorhodospira halophila* bacterium, and mediates the bacterium's negative phototactic response as a reaction to irradiation with blue light (i.e., the microorganism tends to navigate to an environment which is less strongly illuminated) [1]. An intriguing fact is that the very initial photoresponse, at a molecular level, relates to an ultrafast (femtosecond to picosecond scale) isomerisation mechanism [2]—very similar to retinal photoisomerisation in the visual process [3].

PYP has been studied extensively over the past few years, resulting in a detailed picture of the various steps of the protein's photocycle which covers an overall time scale of seconds (for several recent reviews, see e.g., Refs. [4–9]). The experimental [2,10–24] and theoretical [25–35] studies which specifically address the very initial step of the photocycle have confirmed the picture of an ultrafast process (several hundred femtoseconds), while raising a number of controversial issues regarding the electronic states and geometries involved. In addition, the role of the protein environment in creating specific, "optimal" conditions for the isomerisation has not been clarified as yet, despite various efforts [12,21,24,33,34,36–41]. Recent experimental results for various analogs of the chromophore in solution [42–50],

* Corresponding author at: Département de Chimie, Ecole Normale Supérieure, 24 rue Lhomond, F-75231 Paris Cedex 05, France.
Tel.: +33 1 44 32 33 38; fax: +33 1 44 32 33 25.
E-mail addresses: evgeniy.gromov@pci.uni-heidelberg.de (E.V. Gromov), irene.burghardt@ens.fr (I. Burghardt).

1010-6030/$ – see front matter © 2007 Elsevier B.V. All rights reserved.
doi:10.1016/j.jphotochem.2007.04.033

crystalline phase [51] and in the gas phase [21,52–55] offer extensive information that is yet to be explored, complementary to the observations made for the native protein.

Among the key factors influencing the isomerisation event are both the chromophore's intrinsic properties and the influence of the environment (protein or solvent). This includes notably (i) the anionic nature of the chromophore [48], (ii) the chemical nature of the thio-ester moiety, which has been compared in a recent series of experiments [8,46,49,50] with both oxygen and nitrogen containing analogs (see also our previous theoretical study of Ref. [56]), (iii) the presence of hydrogen bonds which stabilize the phenolate moiety of the anionic chromophore [27,38], (iv) the presence of the Arg52 "counter-ion" in the protein environment [33,37]. We have analyzed several of these factors in our previous work; in particular, Ref. [57] unravels the various influences which create the unique electronic structure of the chromophore in its native protein environment. However, our previous studies were limited to the Franck-Condon geometry and did not yet address the twisted geometry (or geometries) of the chromophore that are relevant for the isomerisation. The purpose of the present work is therefore to study various of the above factors in view of their role in the isomerisation process. Like in our previous studies, we use high-level *ab initio* techniques, in particular the CC2 (second-order approximate coupled-cluster singles and doubles) method [58].

As will be shown below, the anionic nature of the chromophore is a determining factor on several accounts: (i) In the anion, the first excited π–π^* state (S_1) is effectively isolated, in contrast to the situation in the neutral species which exhibits close-lying S_1 and S_2 states (this remarkably simple picture is found to persist in the protein [57]). (ii) Despite the simplicity of this electronic structure picture, the isomerisation process is complicated by the fact that two torsional pathways arise in the anionic species: first, torsion around the double bond which is conjugated with the aromatic ring (denoted β in the following) and second, torsion around the single bond adjacent to the aromatic ring (denoted α in the following) [20,27,33]. Two S_1 minima are shown to exist (referred to as $S^{\alpha}_{1,\min}$ and $S^{\beta}_{1,\min}$, respectively), which exhibit twisted geometries with respect to one or the other torsion angle. These observations confirm previous results obtained by Groenhof et al. [33]. The α-torsion has also been previously invoked to explain experimental data [16,20,59]. The two photoinduced torsional pathways are a result of the partially quinone-like electronic structure properties of the anionic chromophore in the ground state. We characterize the corresponding charge distributions and show that a substantial charge shift and "polarization effect" is entailed by the twisting process (increasing charge separation when moving towards the twisted structure).

As suggested in Ref. [33], the relative importance of these two torsional pathways can be strongly influenced by the environment. In particular, the relative energetic position of the two minima, and their position with respect to the nonadiabatic coupling (conical intersection) region will play a key role for the dynamical process. Here, we will comment specifically upon the influence of the hydrogen bonds stabilizing the phenolate moiety, and of the Arg52 residue which plays the role of a counter-ion in the protein environment.

Furthermore, we show that the chemical nature of the ester moiety (containing sulfur, as in the native species, or else oxygen or nitrogen) exerts a significant influence. In the case of the thioester species (–(C=O)–S–), the $S^{\beta}_{1,\min}$ minimum is associated with an S_1–S_0 energy gap of ~0.4 eV, while the corresponding minimum of the amide species (–(C=O)–N–) is located in the immediate neighborhood of a conical intersection. These observations are expected to have an important effect upon the dynamical properties. Indeed, recent experiments [19,49,50] in solution show that an ultrafast *trans–cis* conversion is observed in the amide species whereas the *cis* form is not observed for the sulfur-containing compound [48,50]. While no complete analysis is given here – and we do not address the solution-phase case in this work – we propose a number of elements that will play a role in the unraveling of the experimental observations.

Fig. 1 shows the various molecular species that are addressed in this work, along with the abbreviations that are used.

The remainder of the paper is organized as follows: Section 2 addresses the computational methods used. In the subsequent sections, three aspects will be successively addressed: the char-

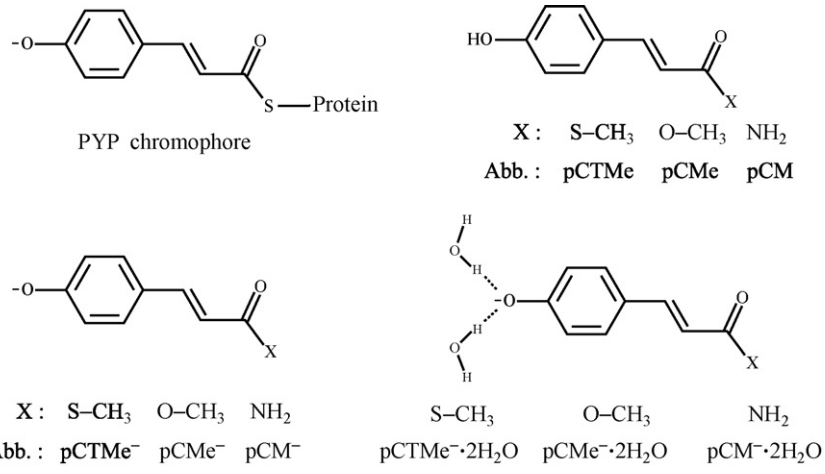

Fig. 1. Chemical structure of the PYP chromophore and its analogs considered in the present study.

acteristic features of the anionic chromophore as compared with its neutral counterpart (Section 3), the twisted configurations of the chromophore (Section 4), the chemical nature of the ester moiety (Section 5), and certain aspects regarding environmental effects (Section 6). Finally, Section 7 concludes.

2. Computational procedures

The work reported here relies for the most part on the second-order approximate coupled cluster (CC2) approach [58], and in part on the more accurate equation-of-motion coupled cluster singles and doubles (EOM-CCSD) method [60–62]. The EOM-CCSD method is characterized by a fairly high accuracy (the maximum error is ∼0.4 eV) [63] with moderate computational costs and is used in this work to verify results of the less accurate CC2 approach. It is a robust and useful tool to study excited states of medium-size molecules (for recent applications, see Refs. [55,56,64]) with the possibility to perform geometry optimization, vibrational analysis and to evaluate various properties of excited states. EOM-CCSD calculations are, however, time-consuming and critical to computational resources for larger systems. For molecules with more than 20 atoms they quickly become a formidable task. An alternative is represented by the CC2 approach [58] which is somewhat less accurate than EOM-CCSD (the maximum error is up to 0.9 eV) [63] but requires much less computational effort. In combination with the resolution-of-the-identity (RI) approximation (for the evaluation of the electron-repulsion integrals) [65,66], one can address considerably (two to three times) larger systems with CC2 than with the presently available EOM-CCSD method. Like the latter method, CC2 allows for computing various ground and excited state properties (oscillator strengths, dipole moments, charge distribution) and for studying effects of geometry relaxation. Both CC2 and EOM-CCSD possess the size-consistency property (important for reaction energies) and can be used in large-scale routine calculations.

In the present study we make use throughout of the CC2 method, for treating the ground and excited states of the PYP chromophore and related species. The method proves to properly describe most of the excited states, and in particular the π–$\pi^*(S_1)$ state to be addressed in detail below. A full geometry optimization for the ground state and the π–π^* excited state was carried out, using analytical gradient techniques. The threshold of convergence used in the geometry optimization procedure (maximum norm of Cartesian gradient) was $<10^{-3}$.

The CC2 calculations with the RI approximation (RI-CC2) were performed employing the TURBOMOLE program package [67]. The EOM-CCSD method was used as implemented in the ACES II ab initio suite of programs [68]. The correlation consistent valence polarized double-ζ basis set (cc-pVDZ) [69] is employed throughout in the coupled-cluster calculations. Diffuse functions were found to have a small influence on the excited states considered here, even in the case of deprotonated (anionic) species (a lowering of 0.2 eV was observed on average for the excitation energies upon changing to the aug-cc-pVDZ basis set). We will be also interested in the first ionization potential (IP) of the PYP chromophore analogs which is evaluated with the outer-valence Green's function (OVGF) method [70]. The IP was found to be sensitive to the presence of diffuse functions in the basis set (ignoring diffuse functions results in an IP value that is about 0.5 eV lower). Therefore, the aug-cc-pVDZ basis set [71] was used to evaluate the IP. The latter calculations were performed with the GAUSSIAN program package [72].

We conclude this section with a note on the application of time-dependent density functional theory (TDDFT), which has been increasingly applied over the past few years for computing excited states of various molecular systems (for recent applications see for example Ref. [73]). The success of the method is related to the low computational cost of TDDFT as compared with wavefunction-based (ab initio) methods, which makes it very attractive in studying polyatomic molecules. One should, however, be cautious when using the TDDFT method as it can give poor predictions in certain cases. The known failures of the method are spatially extended and charge-transfer (CT) excited states (see Ref. [74] and references therein) which are often encountered in large-sized molecules. As our previous study showed [56], excited states of the CT type exist in *p*-coumaric acid (pCA) and *p*-coumaric thio acid (pCTA) and should be anticipated in other analogs of the PYP chromophore. One of these states (π–π^*) turns out to be the state of interest, i.e. the state that is primarily populated upon photon absorption and is expected to be involved in the isomerisation process [56]. De Groot et al. recently showed that conventional TDDFT with the BP86, B3LYP and BHLYP functional gives a wrong ordering of this state in the methyl-oxy-ester of pCA [75]. In view of the above, the TDDFT method cannot be recommended for studying the excited states of the PYP chromophore.

3. Deprotonated versus neutral chromophore

The active form of the native PYP chromophore is the deprotonated (anionic) species (Fig. 1). The role of deprotonation has been intensely discussed in the recent literature, regarding its influence on the tuning of the absorption energy [42,76,77] and on the various steps of the photocycle [78]. It is generally accepted that deprotonation results in a substantial red shift of the chromophore's absorption band, i.e., the energy of the corresponding excited state is lowered. In various experimental works [42,76,77] the energy shift caused by deprotonation was estimated to be about 0.5–0.6 eV. However, our calculations predict a considerably larger value, of about 1.4 eV (see below).

The pronounced effect of deprotonation upon the excitation energy must be due to changes in the electronic structure of the chromophore, as a result of the presence of the negative excess charge, and the redistribution of this charge. While the negative charge is mainly localized on the phenolate moiety in the ground state of the anion, it is conjectured that a hybrid electronic structure exists which combines the phenolic and quinone-like configurations [79], as shown in Fig. 2. This should lead to a partial delocalization of the negative charge, resulting in its stabilization.

To provide more detailed insight into the differences between the anionic and neutral chromophores and the influence of depro-

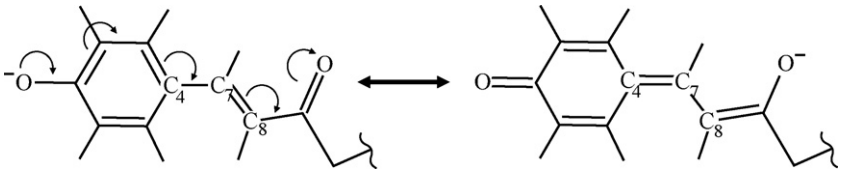

Fig. 2. Phenolic (left) and quinonic (right) resonance structures for the deprotonated anionic chromophore.

tonation on the electronic structure, we compare in Fig. 3 the patterns of the valence molecular orbitals (MO) of the deprotonated and protonated species. The figure shows several highest occupied (HO) and lowest unoccupied (LU) MOs of the neutral and deprotonated *para*-coumaric methyl thio-ester species, i.e., pCTMe and pCTMe$^-$, respectively. These are the principal MOs involved in the low-lying electronic transitions of these systems.

Fig. 4 gives an overview of the relevant electronic states and their energies, for the neutral versus anionic species; Tables 1–3 provide complementary information.

In the following, we briefly recapitulate the properties of the neutral pCTMe chromophore, as detailed in our previous study of Ref. [56]. Following this, the anionic pCTMe$^-$ species will be addressed in some detail.

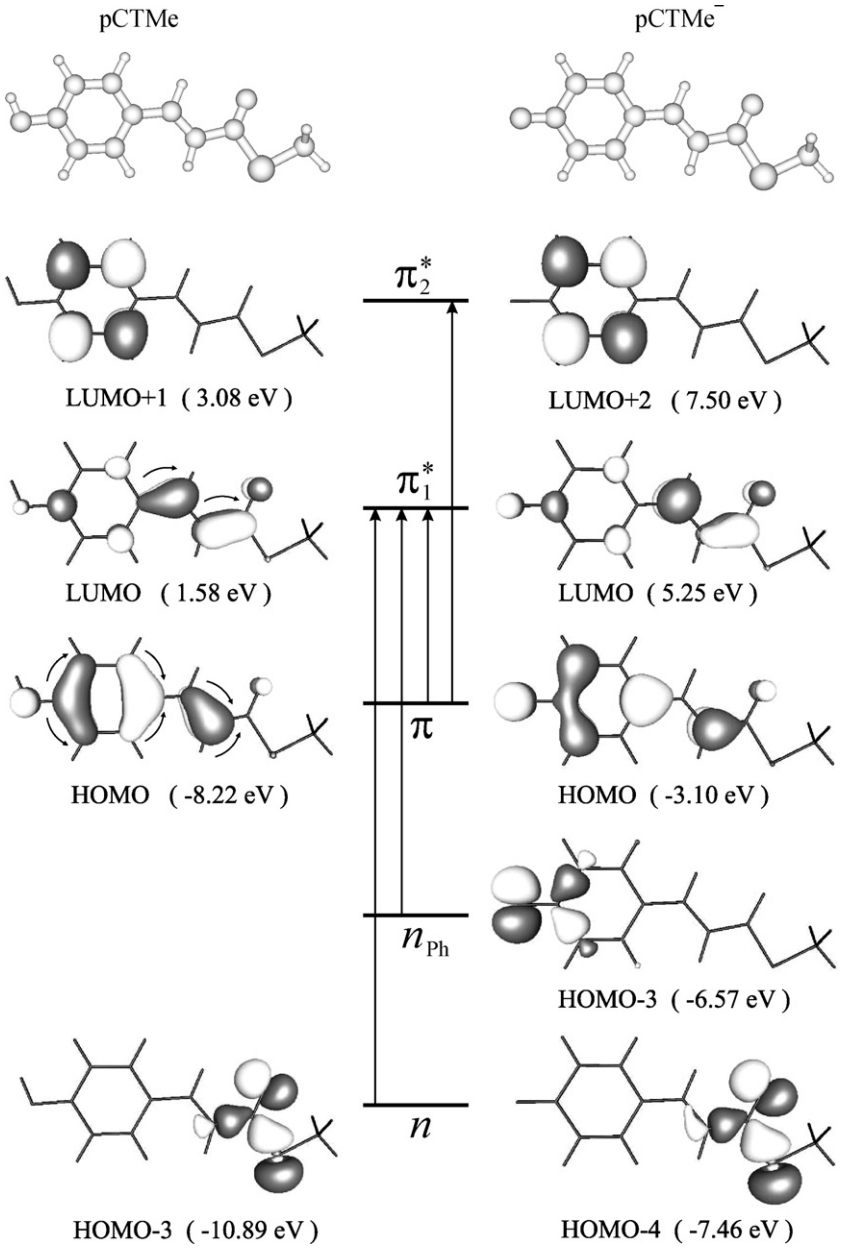

Fig. 3. Relevant Hartree-Fock valence molecular orbitals and principal electronic configurations for the low-lying excited singlet states of the isolated neutral (pCTMe) and isolated anionic (pCTMe$^-$) chromophores at the ground-state equilibrium geometry.

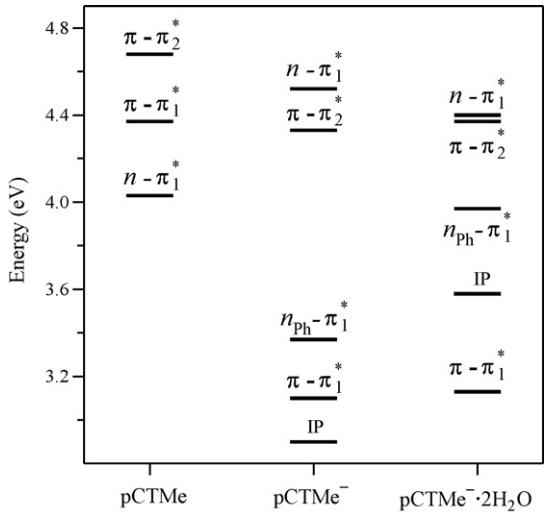

Fig. 4. Diagram showing vertically excited states of pCTMe, $pCTMe^-$ and $pCTMe^-\cdot 2H_2O$. For $pCTMe^-$ and $pCTMe^-\cdot 2H_2O$ the first ionization potential (IP) is given. The diagram is based on the excitation energies given in Table 2; the IP value is from Table 3.

Table 1
Selected bond lengths (Å) and α, β dihedral angles (°) for pCTMe, $pCTMe^-$ and $pCTMe^-\cdot 2H_2O$ at their equilibrium geometries of the ground state

Bond/Angle	pCTMe	$pCTMe^-$	$pCTMe^-\cdot 2H_2O$
O_1–C_1	1.367	1.267	1.295
C_1–C_2	1.409	1.462	1.447
C_2–C_3	1.403	1.387	1.391
C_3–C_4	1.415	1.434	1.429
C_4–C_5	1.420	1.436	1.430
C_5–C_6	1.398	1.386	1.389
C_6–C_1	1.413	1.466	1.451
C_4–C_7	1.463	1.426	1.434
C_7–C_8	1.364	1.391	1.384
C_8–C_9	1.481	1.442	1.451
C_9–O_2	1.234	1.241	1.239
C_9–S	1.806	1.864	1.849
S–C_{10}	1.817	1.816	1.816
$H_1\cdots O_1$			1.782
$H_2\cdots O_1$			1.782
$\angle\alpha$	180.0	180.0	−180.0
$\angle\beta$	180.0	180.0	180.0

3.1. Neutral chromophore

As was found in our previous investigation [56], the neutral chromophore features two π–π* states, with excitations on the conjugated double bond (π–π_1^*) and the phenolic ring (π–π_2^*), respectively. In addition, an n–π* state appears, involving an excitation on the carbonyl moiety as well as the $3p_x$ and $3p_y$ atomic orbitals of sulfur. This state is in fact the lowest-lying excited state of the neutral species [56].

The two π–π* states are found to substantially mix, so that their electronic structure is in general described by linear combinations of the π–π_1^* and π–π_2^* configurations [80]. When the mixing is small, the π–π_1^* configuration can be identified as hav-

Table 2
Vertical transition energies (eV) and oscillator strength in parentheses (a.u.) for the low-lying excited singlet states of pCX, pCX^- and $pCX^-\cdot 2H_2O$ (X = TMe, Me and M)

System	Method	$^1A''(n$–$\pi_1^*)$	$^1A'$ (V)/π–π_1^*	$^1A'$ (V′)/π–π_2^*	$^1A''$ (n_{ph}–π_1^*)
pCTMe					
	CC2	4.03 (<10^{-3})	4.37 (0.939)	4.68 (0.091)	
	EOM-CCSD	4.19 (<10^{-3})	4.60 (0.562)	4.76 (0.419)	
$pCTMe^-$					
	CC2	4.52 (<10^{-3})	3.10 (1.234)	4.33 (0.081)	3.37 (<10^{-3})
	EOM-CCSD	4.67 (<10^{-3})	3.17 (1.237)	4.49 (0.055)	3.98 (<10^{-3})
$pCTMe^-\cdot 2H_2O$					
	CC2	4.40 (<10^{-3})	3.13 (1.196)	4.37 (0.053)	3.97 (<10^{-3})
pCMe					
	CC2	4.88 (<10^{-3})	4.59 (0.478)	4.77 (0.422)	
	EOM-CCSD	5.13 (<10^{-3})	4.94 (0.744)	4.68 (0.103)	
$pCMe^-$					
	CC2	5.36 (<10^{-3})	3.27 (1.068)	4.28 (0.089)	3.49 (<10^{-3})
	EOM-CCSD	5.55 (<10^{-3})	3.35 (1.104)	4.43 (0.061)	4.12 (<10^{-3})
$pCMe^-\cdot 2H_2O$					
	CC2	5.26 (<10^{-3})	3.34 (1.053)	4.35 (0.064)	4.16 (<10^{-3})
pCM					
	CC2	4.48 (<10^{-3})	4.82 (0.542)	4.61 (0.301)	
	EOM-CCSD	4.80 (<10^{-3})	5.01 (0.717)	4.68 (0.071)	
pCM^-					
	CC2	4.89 (<10^{-3})	3.30 (1.011)	4.26 (0.093)	3.57 (<10^{-3})
	EOM-CCSD	5.12 (<10^{-3})	3.39 (1.029)	4.40 (0.065)	4.17 (<10^{-3})
$pCM^-\cdot 2H_2O$					
	CC2	4.81 (<10^{-3})	3.40 (0.978)	4.33 (0.069)	4.24 (<10^{-3})

Table 3
Calculated 1st ionization potential (IP, eV) and vertical transition energy (eV) to the $S_1(\pi–\pi^*)$ excited state for pCTMe, $pCTMe^-$ and $pCTMe^-\cdot 2H_2O$. The aug-cc-pVDZ basis set was used to obtain these results in view of sensitivity of the IP to the presence of diffuse functions (see details in Section 2)

	pCTMe	$pCTMe^-$	$pCTMe^-\cdot 2H_2O$
IP	7.91	2.90	3.58
$S_1(\pi–\pi^*)$	4.15	2.91	2.96

ing by far the dominant oscillator strength (see Table 2) [81]. We will use this criterion where possible in order to distinguish between these states.

As shown in our previous work [56], the ground state of the neutral chromophore exhibits a moderate dipole moment (charge separation), with somewhat more negative charge on the alkene part. The $\pi–\pi_1^*$ transition was found to result in a further charge transfer from the phenol ring to the alkene part of the chromophore [56]. This charge migration trend can also be inferred from the pattern of the π_1^* orbital (Fig. 3) whose electronic density is clearly distinct from the π orbital density. The $n–\pi_1^*$ transition leads to a charge transfer as well, in a direction which is reversed as compared with the $\pi–\pi_1^*$ transition. Finally, the $\pi–\pi_2^*$ transition gives rise to a charge distribution which is similar to the ground state.

We conclude this section with some comments on the quality of the CC2 method in describing the states in question. In fact, the mixing of the $\pi–\pi_1^*$ and $\pi–\pi_2^*$ states makes it difficult to correctly describe their electronic structure. As can be seen from Table 2, there is not always good agreement between the predictions of the CC2 and EOM-CCSD methods regarding the $\pi–\pi^*$ states. Despite the relatively high accuracy of the CC2 method, this method tends to underestimate the state mixing, as follows from a comparison of the oscillator strengths obtained at the CC2 versus EOM-CCSD levels. In contrast to CC2, the EOM-CCSD method predicts a strong mixing of the $\pi–\pi^*$ states at the Franck-Condon geometry, which manifests itself in nearly equal oscillator strengths for both $\pi–\pi^*$ transitions [82]. Furthermore, the CC2 method produces nonuniform deviations: in particular, the CC2 excitation energies deviate by 0.23 eV from the EOM-CCSD estimate for the $\pi–\pi_1^*$ state, but only by 0.08 eV for the $\pi–\pi_2^*$ state; this leads to an underestimation of the energy gap by a factor of almost 2. As for the $n–\pi_1^*$ state, both methods are consistent in predicting that this state is the lowest excited state, and confirm that the $n–\pi_1^*$ transition has a very low oscillator strength. The CC2 versus EOM-CCSD difference in the excitation energy is 0.16 eV in this case.

3.2. Deprotonated chromophore

Deprotonation has a profound effect on the electronic structure properties, on several accounts: (i) all excited states of the anionic species are autoionizing, i.e., metastable with respect to electron detachment (see the ionization potential indicated in Fig. 4 and Table 3); (ii) A new low-lying electronic state of $n–\pi^*$ character appears (denoted as $n_{ph}–\pi_1^*$), whose electron density is localized on the n_{ph} (non-bonding) lone pair of the phenolic oxygen; (iii) the relative energies of the $\pi–\pi_1^*$, $\pi–\pi_2^*$, and $n–\pi_1^*$ states, which were already present in the neutral species, change considerably. These aspects are illustrated in Figs. 3 and 4. We note that the excited state energies of the isolated anionic species (Fig. 4, Tables 2 and 3) are only well-defined within the limits of the lifetime broading with respect to autoionization [83] (see below).

Importantly, the $\pi–\pi_1^*$ state, which is the state predominantly involved in the isomerisation, becomes the anion's lowest-lying excited state and is well separated from the $\pi–\pi_2^*$ state. The mixing of the $\pi–\pi^*$ states is therefore negligible in the deprotonated species and one can readily distinguish the $\pi–\pi_1^*$ and $\pi–\pi_2^*$ states by their oscillator strength. Furthermore, the electronic structure of the $\pi–\pi_1^*$ and $\pi–\pi_2^*$ states is now well described by the CC2 method, as proven by the good agreement of the CC2 and EOM-CCSD results (Table 2). The largest deviation is observed for the $\pi–\pi_2^*$ state (0.16 eV) whose electronic structure involves doubly excited configurations [84]. Despite this satisfactory agreement, the shortcomings of the CC2 method are manifest, e.g., in the characterization of the new $n_{ph}–\pi_1^*$ excited state, which is not adequately described (see Table 2): The energy of this state is underestimated by about 0.6 eV. Still, we consider the use of the CC2 method as an appropriate strategy, given that most of the following discussion focusses upon the $\pi–\pi_1^*$ state.

In the native protein environment, the $\pi–\pi_1^*$ state remains the first excited state and is again quasi-isolated [85]. Disregarding the issue of autoionization, the electronic character of the chromophore in the protein environment remains rather close to the isolated anion [57]. It is therefore worth considering the electronic structure of the anionic chromophore in some detail (see below).

Finally, we comment upon the fact that the excited states of the anionic species are autoionizing, i.e., metastable with respect to electron detachment. This in principle requires an appropriate electronic structure treatment, using complex absorbing potentials (CAPs) [86]. On the other hand, the autoionizing nature of the states can be looked upon as an artifact of considering the anionic species in isolation. Indeed, the ionization potential is considerably raised in the native protein environment or in solution. As we have shown in Ref. [57], the positively charged Arg52 amino acid which acts as a counter-ion with respect to the chromophore induces a twofold increase of the IP. Likewise, the hydrogen-bond forming amino acids lead to an important increase of the IP.

3.3. Neutral versus deprotonated chromophore: orbital patterns

As can be seen from Fig. 3, deprotonation results in marked changes in the π and π_1^* orbital patterns, while the π_2^* and n orbitals are unchanged. We first address the changes occurring in the π (HOMO) and π_1^* (LUMO) orbitals, which are of key importance for the isomerisation process. By comparing the patterns of the HOMO and LUMO of the neutral versus anionic species, one can infer a systematic change in the electronic density that apparently corresponds to a charge shift from the phenolate moiety to the alkene part. This charge migration trend is indicated

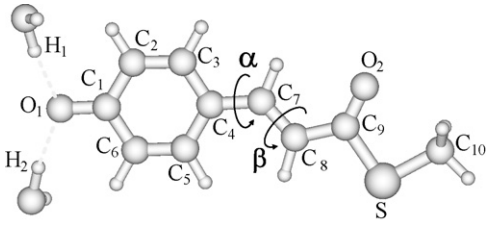

Fig. 5. Molecular structure of $pCTMe^{-}\cdot 2H_2O$ at the $S_{0,eq}$ point along with the numbering of the atoms and short notations for the twisting processes (α-twist around the C_4–C_7 bond, β-twist around the C_7=C_8 bond) which are used throughout in the text and tables. A similar spatial structure corresponds to the $S_{1,TS}$ point (see differences in Table 6).

by arrows in Figs. 2 and 3, and would eventually result in a quinone type structure for the anionic species. This shift entails, in particular, that the π-bonding structure of the C_7=C_8 bond is to some extent lost, while some π-bonding character appears in the C_4–C_7 bond adjacent to the aromatic ring (Table 1, see Fig. 5 for the numbering of the atoms). The charge shift is accompanied by significant changes in the bond lengths (indicating a partial formation of the quinone structure): notably, the C_1–C_6 and C_1–C_2 bonds acquire partial single-bond character (elongation by 0.05 Å) as does the C_7=C_8 bond (elongation by 0.03 Å). Conversely, the C_4–C_7 bond acquires partial double-bond character (contraction by 0.04 Å). Interestingly, there is also a conspicuous increase of the C_9–S bond length. This is in fact an indication of the charge migration to the chromophore's alkene fragment.

Despite the tendency towards a quinone-like structure of the HOMO orbital, the electronic ground state of the anion features significantly more negative charge density on the phenolate moiety (−0.62) than on the alkene fragment (−0.38). At the same geometry, the S_1 charge distribution is −0.5 (phenolate moiety) versus −0.5 (alkene moiety), indicating a charge shift towards the alkene part. The difference in S_0 versus S_1 dipole moments is $\Delta\mu = |\vec{\mu}_{S_1} - \vec{\mu}_{S_0}| = 3.1$ D.

As can be seen from Fig. 3, all orbitals experience an increase in energy, which is largest for the π MO (about 5.1 eV). One can therefore expect changes in the excitation energies for all transitions involving this MO. In particular, the π–π_1^* transition is considerably lowered in energy, to the extent that the π–π_1^* state becomes the lowest excited state. This can alternatively be interpreted in terms of the stabilizing effect of the charge transfer associated with this transition, i.e. the π–π_1^* transition is more favorable in the anionic species than in the neutral chromophore, since it results in a delocalization of the negative charge (while the same charge migration trend leads to a localization in the neutral chromophore, since the alkene part is slightly negatively charged [56]).

3.4. The hydrogen-bonded $pCTMe^{-}\cdot 2H_2O$ species

In view of the hydrogen bonding effects present in the native protein environment [57] which stabilize the $S_1(\pi$–$\pi_1^*)$ excited state against autoionization we will focus in the following upon an anionic species containing hydrogen bonds with two water molecules, i.e. the $pCTMe^{-}\cdot 2H_2O$ species (Fig. 5). As can be seen from Table 3 and Fig. 4, the IP of this complex lies 0.7 eV higher than that of the isolated chromophore, so that the first excited state is located below the ionization threshold. The other excited states still lie in the ionization continuum, see Fig. 4. Apart from the rise of the IP, there is a pronounced increase in energy of the n_{ph}–π_1^* excited state (Table 2). This is clearly the effect of the hydrogen bonding—very similarly to the effect of the hydrogen bonds to the Tyr42 and Glu46 amino acids in the native protein environment [57].

Hydrogen bonds to the phenolic oxygen thus have a twofold effect in that they (i) act so as to raise the ionization potential, thus stabilizing the system against autoionization, and (ii) change the energetics. With regard to (ii), hydrogen bonds in fact provide a sensitive measure of the chromophore's charge distribution, in that they stabilize the states which exhibit a localized charge distribution on the phenolate moiety. This is the case for the S_0 ground state at the Franck-Condon geometry, and for certain twisted geometries addressed in the next section. A more detailed account of this aspect is given in Section 4.

4. Twisted S_1 configurations of the chromophore

As explained above, the present discussion addresses the $pCTMe^{-}\cdot 2H_2O$ species, whose $S_1(\pi$–$\pi_1^*)$ state is stable with respect to autoionization. Most of the following focusses on this excited state; for simplicity of notation, we therefore denote this state as π–π^*.

In this section, we present results of a full geometry optimization for the π–π^* state. Three stationary points are identified on the $S_1(\pi$–$\pi^*)$ potential energy surface: a quasi-planar configuration of the chromophore corresponding to a saddle point ($S_{1,TS}$) and two twisted structures ($S^{\alpha}_{1,min}$ and $S^{\beta}_{1,min}$), with respect to either the C_4–C_7 bond (formally a single bond) or else the C_7=C_8 bond (formally a double bond). In the following, we successively address these three structures (Section 4.1). Various data relevant for the discussion are reported in Tables 4–7.

The existence of a twisted excited-state structure with respect to the C_4–C_7 single bond which is adjacent to the aromatic ring may first seem surprising. Its appearance is connected to the particular electronic structure properties of the anionic species in the ground state, i.e., its partial quinone-like character (Section 3). The existence of such a twisted structure has been suggested previously [20,27,33], but no explicit characterization of this structure has been performed so far. Below we will comment in

Table 4
Ground state (S_0) and excited state (S_1) permanent dipole moments (D) and their difference $\Delta\mu = |\vec{\mu}_{S_1} - \vec{\mu}_{S_0}|$ (D) for the $pCTMe^{-}\cdot 2H_2O$ species at the different stationary points. Only dipole moments within a given geometry can be compared[a]

	$S_{0,eq}$	$S_{1,TS}$	$S^{\alpha}_{1,min}$	$S^{\beta}_{1,min}$
S_0	8.8	8.7	11.6	2.1
S_1	2.9	1.6	5.4	11.7
$\Delta\mu$	6.0	7.1	16.9	12.5

[a] The dipole moment for a charged system depends on the origin and orientation (geometry) of the system. The origin for the species discussed in the table is at their center of mass. Comparison of the dipole moments at the different stationary points is not meaningful since the molecular geometries are different.

Table 5
Ground and excited state integrated Mulliken charge distributions (calculated using CC2 density matrices) partitioned between the chromophore ring and alkene part for the pCTMe$^-$·2H$_2$O chromophore at different stationary points

	$S_{0,eq}$		$S_{1,TS}$		$S^{\alpha}_{1,min}$		$S^{\beta}_{1,min}$	
	S_0	S_1	S_0	S_1	S_0	S_1	S_0	S_1
Chromophore ring	−0.71	−0.53	−0.71	−0.51	−0.87	−0.25	−0.39	−0.76
Alkene part	−0.29	−0.47	−0.29	−0.50	−0.13	−0.75	−0.61	−0.24

Table 6
Selected bond lengths (Å) and α, β dihedral angles (°) for pCTMe$^-$·2H$_2$O at the different stationary points

Bond/Angle	$S_{0,eq}$	$S_{1,TS}$	$S^{\alpha}_{1,min}$	$S^{\beta}_{1,min}$
O_1–C_1	1.295	1.319	1.296	1.308
C_1–C_2	1.447	1.441	1.446	1.443
C_2–C_3	1.391	1.404	1.391	1.394
C_3–C_4	1.429	1.422	1.435	1.435
C_4–C_5	1.430	1.428	1.431	1.435
C_5–C_6	1.389	1.408	1.392	1.393
C_6–C_1	1.451	1.433	1.447	1.445
C_4–C_7	1.434	1.484	1.477	1.424
C_7–C_8	1.384	1.404	1.428	1.464
C_8–C_9	1.451	1.439	1.412	1.456
C_9–O_2	1.239	1.256	1.260	1.234
C_9–S	1.849	1.870	1.921	1.848
S–C_{10}	1.816	1.815	1.811	1.816
$H_1\cdots O_1$	1.782	1.820	1.895	1.756
$H_2\cdots O_1$	1.782	1.824	1.893	1.755
$\angle\alpha$	−180.0	180.0	−89.2	−178.6
$\angle\beta$	180.0	179.9	162.5	−89.6

some detail upon the characteristics of this structure as compared with the structure resulting from a twist with respect to the C_7=C_8 double bond.A number of observations will be made regarding the evolution of the charge distributions as a function of geometry. These observations include a polarization effect when moving towards the twisted geometry, and a charge inversion in the S_0 and S_1 states at the twisted geometries.

4.1. Stationary structures

4.1.1. $S_{1,TS}$ stationary point

The first stationary point obtained by allowing structural relaxation from the FC geometry corresponds to a quasi-planar geometry of the chromophore, i.e. no twist occurs (Fig. 5). We denote this stationary structure $S_{1,TS}$, since it corresponds to a saddle point (transition state) with respect to the torsion around the C_4–C_7 bond. (That is, $S_{1,TS}$ separates two symmetrically disposed minima – denoted $S^{\alpha}_{1,min}$ below – that result from clockwise or counterclockwise rotation around the C_4–C_7 bond.) The saddle point character of the $S_{1,TS}$ geometry is consistent with the observations of Ref. [27]. Relaxation to the $S_{1,TS}$ geometry involves alterations of the bonds and valence angles of the pCTMe$^-$·2H$_2$O complex, and leads to an energetic lowering by 0.11 eV. The process is characterized by a moderate elongation of the C_4–C_7, C_7=C_8, C_9–O_2 and C_9–S bonds (Table 6).

An interesting observation concerns an elongation of the hydrogen bonds, by about 0.04 Å as compared with the $S_{0,eq}$ geometry (Table 6). This indicates a reduction of the electron density (negative charge) on the phenolate oxygen in the S_1 state as compared to the ground state. This trend is consistent with the charge distribution properties discussed in Section 3, i.e., the S_1 state features a marked delocalization of the negative charge towards the alkene moiety.

4.1.2. Twisted structure with respect to the C_4–C_7 bond

As has been noted above, the $S_{1,TS}$ structure is a saddle point with respect to torsion around the C_4–C_7 bond [27]. Relaxation with respect to torsion leads to the stationary point $S^{\alpha}_{1,min}$, with an $\alpha(C_3C_4C_7C_8)$ twist angle of $\alpha = -89.2°$ (Fig. 6) [87]. This confirms and extends the finding by Groenhof et al. [33] that in the isolated anionic chromophore, a barrierless path leads from the Franck-Condon geometry to the single-bond twisted minimum [88].

As already mentioned, both the existence of the single-bond twisted minimum and the fact that the system spontaneously evolves towards this minimum are surprising. We attribute this to the partial double-bond character of the C_4–C_7 bond. Given that the HOMO of Fig. 3 reflects the partial formation of a C_4–C_7 double bond while the LUMO is non-bonding, torsion is favorable in the excited state—very similarly to the situation for a true double bond. Clearly, the partial quinone-like character of

Table 7
Relative changes of the ground state (S_0) and excited state (S_1) energies (eV) and absolute values of the S_1–S_0 energy gap (eV) for pCM$^-$·2H$_2$O, pCMe$^-$·2H$_2$O and pCTMe$^-$·2H$_2$O at the different stationary points

	pCM$^-$·2H$_2$O			pCMe$^-$·2H$_2$O			pCTMe$^-$·2H$_2$O		
	S_0	S_1	S_1–S_0	S_0	S_1	S_1–S_0	S_0	S_1	S_1–S_0
$S_{0,eq}$	0.00	3.40	3.40	0.00	3.34	3.34	0.00	3.13	3.13
$S_{1,TS}$				+0.15	−0.13	3.07	+0.14	−0.11	2.88
$S^{\alpha}_{1,min}$	+1.24	−0.26	1.89	+1.23	−0.27	1.84	+1.12	−0.39	1.62
$S^{\beta}_{1,min}$	+2.53	−0.80	0.07	+2.44	−0.72	0.19	+2.16	−0.56	0.42

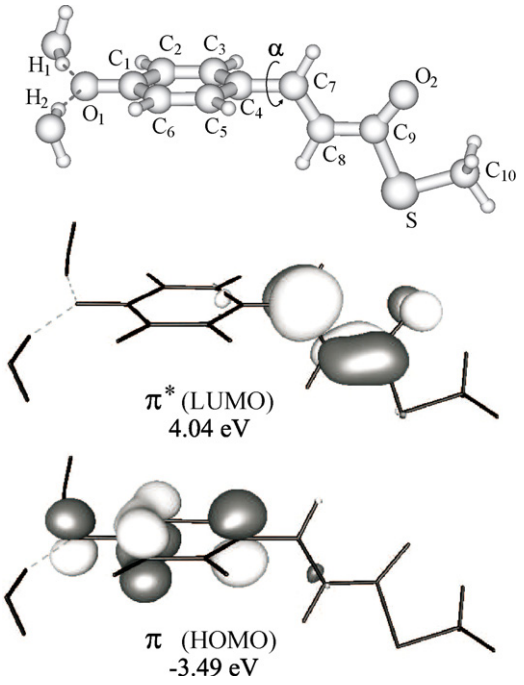

Fig. 6. Molecular structure and patterns of the HOMO and LUMO for $pCTMe^{-}\cdot 2H_2O$ at the $S^{\alpha}_{1,min}$ minimum. In addition, the HOMO/LUMO energies are shown.

the chromophore relates to this second torsional path, besides the double-bond twist.

The $S^{\alpha}_{1,min}$ structure is about 0.28 eV lower in energy than the $S_{1,TS}$ structure and corresponds to a local minimum. The S_0–S_1 energy gap is $\Delta_{S_1-S_0} = 1.62$ eV at $S^{\alpha}_{1,min}$, as compared with $\Delta_{S_1-S_0} = 2.88$ eV at $S_{1,TS}$. As can be seen from Table 6, the $S_{1,\alpha}$ geometry features a slight twist around the C_7=C_8 bond, with a β torsional angle ($C_4C_7C_8C_9$) of $\beta = 162.5°$ versus $\beta = 179.9°$ at the $S_{1,TS}$ geometry. Further, a slight elongation of the C_7=C_8 bond occurs, along with a marked lengthening of the C_9–S bond—a sign of an enhanced migration of the electronic charge to the chromophore's alkene moiety (see below).

Fig. 6 shows the HOMO and LUMO molecular orbital patterns at the $S^{\alpha}_{1,min}$ geometry. Comparison with the MOs at the planar geometry (Fig. 3) shows a certain similarity. Yet, there are noticeable differences, which mainly concern the localization of the HOMO/LUMO electron density on the phenyl versus alkene moiety. In particular, the HOMO density is concentrated primarily on the phenolic part, with a p-type atomic orbital on the C_4 atom (Fig. 6). This is in contrast to the HOMO at the Franck-Condon geometry (Fig. 3) which clearly shows electron density on both the phenyl and alkene parts and exhibits a trend towards the formation of a C_4–C_7 double bond. The LUMO at the $S^{\alpha}_{1,min}$ geometry is seen to have experienced analogous changes: The electronic density is now localized exclusively on the alkene fragment, with a p-type orbital on the C_7 atom. Overall, the new patterns of the HOMO and LUMO exhibit a deconjugation (uncoupling) of the π-electron system, yielding two orthogonal π-electron subsystems localized on the phenyl versus alkene fragments, respectively. This uncoupling effect is a general phenomenon occurring at the twisted geometries of polyenes (see, e.g., Ref. [89]).

As a result of these changes in the HOMO and LUMO patterns, a pronounced change of the charge properties occurs, in that the charge distributions become more "polarized" (see Table 5). While the integrated charges over the phenyl versus alkene moieties in the $S_1(\pi$–$\pi^*)$ excited state correspond to the ratio 0.53:0.47 at the Franck-Condon geometry (and 0.50:0.50 at the $S_{1,TS}$ geometry), the ratio is 0.25:0.75 at the $S^{\alpha}_{1,min}$ geometry. Clearly, a substantial shift of the negative charge towards the alkene part has taken place in the S_1 state. At the same time, the S_0 ground state shows the opposite polarisation, with a charge ratio of 0.87:0.13. This evolution is also reflected in the difference in dipole moments between the S_1 and S_0 states, which increases from $\Delta\mu = |\vec{\mu}_{S_1} - \vec{\mu}_{S_0}| = 6.4$ D at the Franck-Condon geometry to $\Delta\mu = 16.9$ D at the $S^{\alpha}_{1,min}$ geometry (Table 4).

The hydrogen bond lengths again turn out to be a sensitive indicator of the charge properties. Indeed, a further significant lengthening (by about 0.07 Å) is observed. At the $S^{\alpha}_{1,min}$ geometry, the hydrogen bond lengths are thus increased by 0.11 Å as compared with the equilibrium geometry of the ground state. This again reflects that torsion around the C_4–C_7 bond state results in a pronounced S_1 charge transfer from the phenolate oxygen in the direction of the alkene part.

4.1.3. *Twisted structure with respect to the C_7=C_8 bond*

Twisting around the C_7=C_8 bond by an angle $\beta \lesssim 55°$ and allowing for geometry relaxation again leads to the α-twisted minimum, i.e., the $S^{\alpha}_{1,min}$ stationary point addressed in the preceding section. In order to reach the stationary point corresponding to the C_7=C_8 twist ($S^{\beta}_{1,min}$) (Fig. 7) [90], it is necessary to start from a configuration that is already strongly twisted around the C_7=C_8 bond, by at least $\beta \approx 60°$. This indicates that a substantial barrier [91] (located around $\beta \approx 55°$) must exist with respect to the β-torsion, in qualitative agreement with the findings by Groenhof et al. [33].

The relaxation process ends at a torsional angle of $\beta = -89.6°$. The $S^{\beta}_{1,min}$ structure (Fig. 7) that is thus obtained is by 0.17 eV lower in energy than the $S^{\alpha}_{1,min}$ structure. The S_1–S_0 energy gap is $\Delta_{S_1-S_0} = 0.42$ eV, i.e., much smaller than the gap of $\Delta_{S_1-S_0} = 1.62$ eV for the $S^{\alpha}_{1,min}$ structure.

The $S^{\beta}_{1,min}$ stationary point is characterized by torsional angles $\beta = -89.6°$ and $\alpha = -178.6°$. Besides, one can note a further elongation of the C_7=C_8 bond and a marked shortening of the C_4–C_7 and C_9–S bonds as compared with the values at the $S^{\alpha}_{1,min}$ geometry (Table 6). These latter bonds nearly acquire their ground state bond length values. As will become clear below, these changes indicate a charge migration from the alkene fragment "back" to the phenolic part of the chromophore.

Inspection of the HOMO and LUMO orbital patterns (Fig. 7) at the $S^{\beta}_{1,min}$ point shows a deconjugation of the initial π-system, similar to the case of the $S^{\alpha}_{1,min}$ stationary point. The C_7=C_8 π-bond is clearly broken, and the C_7 and C_8 atoms now exhibit orthogonal p-type orbital patterns. From Fig. 7, the HOMO and LUMO orbital patterns are such that the HOMO electronic

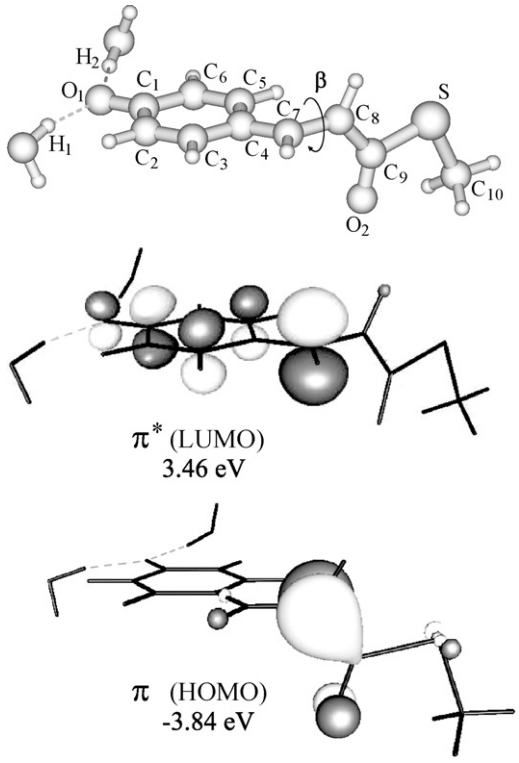

Fig. 7. Molecular structure and patterns of the HOMO and LUMO for pCTMe$^-$·2H$_2$O at the $S^{\beta}_{1,min}$ minimum. In addition, the HOMO/LUMO energies are shown.

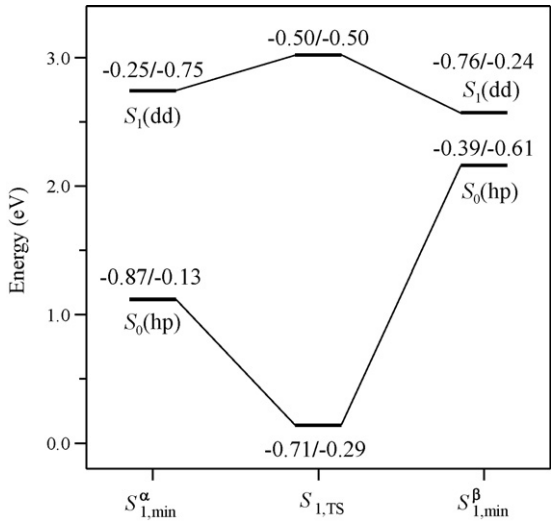

Fig. 8. Diagram showing energies and integrated charge distribution ("phenol part" vs. "alkyl part") for the ground (S_0) and excited (S_1) states of pCTMe$^-$·2H$_2$O at the $S^{\alpha}_{1,min}$, $S_{1,TS}$, and $S^{\beta}_{1,min}$ stationary points. At the $S^{\alpha}_{1,min}$ and $S^{\beta}_{1,min}$ points the electronic configurations of the states are indicated in terms of "dot-dot" (dd) and "hole-pair" (hp) notation (see Section 4.2 for details).

density is concentrated on the alkene part, while the LUMO density is concentrated on the phenolic part. This distribution is inverted as compared with the $S^{\alpha}_{1,min}$ structure. This is borne out by the observed dipole moments (Table 4) and charge distributions (Table 5) which feature a 0.76:0.24 (S_1) ratio for the phenyl versus alkene integrated charges. That is, the S_1 state now exhibits a localization of the negative charge on the phenolate moiety, whereas the S_0 state is of charge transfer character (with a charge ratio 0.39:0.61).

Note that the occurrence of different orbital localization patterns upon twisting around different bonds in conjugated systems was previously reported by Momicchioli et al. (see e.g. Ref. [92] and references therein) as well as by Dekhtyar and Rettig [93].

What is the source of this inversion of the charge character? In the next section we analyze this phenomenon in terms of the biradicaloid state theory developed by Bonačić-Koutecký et al. [94,95] for ethylene and protonated Schiff bases. We further refer to related work by Dekhtyar and Rettig who propose a unified biradicaloid theory for double and single bond twisted geometries [93], partially drawing on the concept of twisted intramolecular charge transfer (TICT) states [96]. The present analysis sheds some light on the previous observations of Ref. [33] which correctly identified the charge distribution at the $S^{\beta}_{1,min}$ minimum, but did not comment upon the evolution of the charge distribution as a function of geometry.

Finally, the above charge transfer trend is again underscored by the evolution of the hydrogen bond lengths. Thus, the $S^{\beta}_{1,min}$ state exhibits substantially shorter hydrogen bonds than those found at the $S^{\alpha}_{1,min}$ structure, with values that are even smaller than at the equilibrium of the ground state (Table 6).

4.2. Interpretation in terms of the biradicaloid state theory

In Fig. 8, we present a diagram summarizing our findings for the charge distributions in the ground (S_0) and excited (S_1) states of the pCTMe$^-$·2H$_2$O chromophore at the three stationary points ($S_{1,TS}$, $S^{\alpha}_{1,min}$ and $S^{\beta}_{1,min}$). Based upon this diagram, we briefly recapitulate: (i) At the $S_{1,TS}$ geometry, the negative charge is predominantly localized on the phenyl moiety in S_0, while a migration of the charge towards the alkene part occurs in $S_1(\pi–\pi^*)$ (leading to a balanced charge distribution in the excited state). (ii) The C_4–C_7 bond twist ($S^{\alpha}_{1,min}$) results in a polarization effect that enhances the localization of the negative charge on the phenyl moiety in S_0, and the localization of the charge on the alkene moiety in S_1. (iii) The C_7=C_8 bond twist ($S^{\beta}_{1,min}$) gives rise to the "inverse" polarization effect, i.e., a localization of the negative charge on the alkene part in S_0, and on the phenyl moiety in S_1. Furthermore, an opposite HOMO versus LUMO localization is observed for the $S^{\alpha}_{1,min}$ versus $S^{\beta}_{1,min}$ geometries, i.e., the HOMO is localized on the donor (phenolate) side for the $S^{\alpha}_{1,min}$ geometry, but on the acceptor (alkene) side for the $S^{\beta}_{1,min}$ geometry (and *vice versa* for the LUMO).

These observations suggest that a biradicaloid model [94,95] for the twisted geometries could explain certain characteristic features of the twisted structures. In the following, we will therefore give a brief perspective on the biradicaloid state theory, following in part previous work by Bonačić-Koutecký et al. [94,95], and the unifying description of single versus double-bond twisted geometries provided by Rettig and collaborators [20,93].

Our starting point is the two-electron two-orbital model as discussed by Bonačić-Koutecký et al. [94,95], which characterizes biradicaloid structures arising at twisted double-bond geometries. The model uses a minimal basis of localized p-orbitals at the atomic centers of the twisted double bond. This localized orbital description is most appropriate at the twisted geometry where the π-bonding structure is lost ("π-decoupling effect"). In extended conjugated systems where the single bonds acquire partial double-bond character, an analogous description holds for single bond twisted geometries [93]. As can be seen from Figs. 6 and 7, the p-orbital description is entirely consistent with the structure of the HOMO and LUMO orbitals both at the $S^{\beta}_{1,\min}$ and, $S^{\alpha}_{1,\min}$ geometries.

Using this minimal model, two-electron configurations are constructed in the localized p-orbital basis. According to Refs. [94,95], the relevant configurations include a "dot-dot" (dd) configuration, with the two electrons occupying different orbitals, and two "hole-pair" (hp) configurations with both electrons occupying one or the other orbital. For polar double-bond systems, two out of these three configurations are generally most relevant for the S_1–S_0 interaction, i.e., the dd (p_{left}–p_{right}) configuration and one of the hp configurations (e.g., p^2_{right}). These features are essentially confirmed by detailed electronic structure calculations for protonated Schiff bases like retinal [97,98]. As shown by Rettig and collaborators, a very similar picture holds for single bonds in twisted stilbenoid systems [93].

The hp and dd configurations are uncoupled at the 90° twisted geometry, but start to mix when moving towards the planar Franck-Condon geometry. The absence of configurational mixing at the twisted geometry accounts for the observed polarization effect, i.e., the observed charge separation and increase in dipole moments. As pointed out in the preceding section, the charge polarization effect is maximal at the 90° twisted geometry. Therefore, the charge separation is more extreme at the $S^{\alpha}_{1,\min}$ and $S^{\beta}_{1,\min}$ geometries as compared with the $S_{1,TS}$ geometry (see Fig. 8). Due to their opposite charge character, transitions between the two relevant configurations will involve an overall shift, or *translocation* of the excess charge. Again, a strong analogy exists with respect to the charge translocation effect observed for retinal and other protonated Schiff bases [94,98], which exhibit a positive excess charge.

When focusing on the twisted bonds, the HOMO/LUMO orbitals of Figs. 6 and 7 can be identified with the p_{left}/p_{right} localized orbitals; hence, one can identify the configurations as follows: hp = $(HOMO)^2(LUMO)^0$, and dd ≡ $(HOMO)^1(LUMO)^1$. This assignment holds for both twisted bonds; however, the hp configuration entails a localisation on the phenyl part for the $S^{\alpha}_{1,\min}$ geometry and a localisation on the alkene part for the $S^{\beta}_{1,\min}$ geometry. The energetic ordering of these configurations will in general depend upon the interplay of the HOMO/LUMO gap and the electron–electron repulsion [93–95].

In Fig. 8, the configurations obtained in our calculations for the $S^{\alpha}_{1,\min}$ and $S^{\beta}_{1,\min}$ geometries are characterized in terms of their dd versus hp character, and the charge distribution over the phenyl/alkene moieties is indicated. At both geometries, the S_1 configuration is found to be dd, while the S_0 configuration is hp. Importantly, the charge localisation is opposite for the $S^{\beta}_{1,\min}$ versus $S^{\alpha}_{1,\min}$ geometries: While the negative charge is localized on the alkene side for the $S^{\alpha}_{1,\min}$ geometry – in conformity with the prevailing S_1 charge distribution – the charge is localized on the phenyl side at the $S^{\beta}_{1,\min}$ geometry. The $S^{\beta}_{1,\min}$ charge distribution is thus "inverted" as compared with the dominant charge character of S_1.

What is the source of this inversion of the charge character at the $S^{\beta}_{1,\min}$ minimum? It is a direct consequence of the HOMO/LUMO localization, which was found to be inverted as compared with the single-bond twist, as pointed out above (i.e., the HOMO is localized on the acceptor (alkene) moiety, while the LUMO is localized on the donor (phenyl) moiety for the $S^{\beta}_{1,\min}$ geometry). This observation is entirely consistent with the general rules proposed by Dekhtyar and Rettig [93] for double-bond versus single bond twists. This localization pattern, in conjunction with the dd/hp energetic ordering determines the charge character of the respective states. Since the small S_1–S_0 energy gap at the $S^{\beta}_{1,\min}$ minimum indicates the vicinity of a conical intersection (in accordance with Ref. [33]), a change of the configuration ordering and an accompanying charge inversion is expected in this region of configuration space. We thus conjecture that the $S^{\beta}_{1,\min}$ geometry is located in a region with an "atypical" S_1 charge distribution, close to this intersection. A similar charge inversion close to the S_1–S_0 conical intersection is observed for retinal type systems, as shown in our recent analysis [99,100] and related work by Robb and collaborators [97] and Martínez and collaborators [98].

5. Influence of α-carbonyl heteroatoms

The nature of the heteroatom bonded to the carbonyl moiety (i.e., sulfur in the case of the native PYP chromophore) potentially plays an important role in the energetics and dynamics of the chromophore. That is, one expects noticeable differences to occur between the thio-ester (–(C=O)–S–CH_3), ester (–(C=O)–O–CH_3), and amide (–(C=O)–N–CH_3) species. Indeed, a series of recent experiments for various chromophore analogs in solution [8,49,50] suggests that the isomerisation behavior strongly depends upon the chemical nature of the α-carbonyl heteroatom. Specifically, the isomerisation yield decreases in the sequence N–O–S, and the formation of a *cis* isomer is in fact only clearly observed for the amide species [49,50]. (In this case, the S_1 decay time scale is in the range of 2.4–4.0 ps [50] as compared with ∼1.9 ps in the native protein [19] and ∼10 ps in the denatured protein [19].) In the following, we will therefore address the effect of the heteroatom on the electronic structure properties described in the preceding sections.

5.1. Franck-Condon geometry: neutral versus anionic species

According to our previous work on the neutral chromophore [56], the most pronounced influence of the heteroatom concerns the non-bonding n molecular orbital, which has a direct partic-

ipation of the heteroatom atomic orbitals. As a result the n–π* state (from here on $\pi^* \equiv \pi_1^*$) turns out to be the lowest-lying excited state in the neutral *p*-coumaric thio acid (CTA) species as well as in the pCTMe ester species. This is in contrast to the oxygen substituted analogs *p*-coumaric acid (CA) and pCMe [56]. In the following, we therefore first detail our findings for the n–π* state, and then turn to the effect of the heteroatom on the π–π* state. This will prepare the ground for the subsequent discussion (Section 5.2) of the heteroatom influence on the isomerisation.

5.1.1. The n–π* state

In Ref. [56], we have carried out a detailed analysis of the role of oxygen versus sulfur in the neutral CTA versus CA chromophores. According to this analysis, the n–π* state is the lowest excited state of the CTA species, but lies almost 1 eV higher in CA, where it turns out to be the third excited state. This enormous difference is due to the higher energy of the n MO in the case of sulfur, and can eventually be traced back to the higher energy of the 3p atomic orbitals (AOs) of sulfur as compared with the 2p AOs of oxygen. This analysis applies in particular to the comparison between pCTMe and pCMe.

In the amide species (pCM), the n MO turns out to be intermediate between the energies of this MO in pCTMe and pCMe. One would therefore expect that the n−π* state in pCM is lower in energy than in pCMe but higher in energy than in pCTMe (Table 2). According to our – very accurate – EOM-CCSD calculation the n−π* state is found to be the second excited state in the pCM species while the CC2 method predicts that the state is the lowest one (Table 2).

In the anionic species, the state ordering changes significantly, as detailed in Section 3. The n–π* state now lies above the π–π_1^*, π–π_2^* and n_{ph}−π* states (Table 2). Still, comparison between the S-, O- and N-substituted species shows that the above trends again hold, i.e., the sulfur substituted species features the lowest-lying n−π* state (Table 2). It is interesting to note that the n−π* state seems to be the second excited state of the chromophore in native PYP. This was established in the experimental study by Borucki et al. [101] and is also supported by our recent investigation [57].

5.1.2. The π–π* state

As can be seen from Table 2, the π–π* state is also affected by the heteroatom, even though to a lesser extent than the n−π* state. Its energy is lowest for the S-substituted chromophore and successively increases for the O- and N-substituted species (Table 2). The red shift of the π–π* state in the presence of sulfur is in a qualitative agreement with the findings of previous experimental studies [42,76]. The observed shift apparently correlates with the stronger electron acceptor properties (electron affinity) of –(C=O)–S–CH_3 as compared with those of –(C=O)–O–CH_3 and –(C=O)–NH_2. This is also in agreement with the somewhat higher IP of the S-substituted chromophore as compared with the O- and N-substituted species (i.e., for $pCTMe^-$, $pCMe^-$ and pCM^- the respective IPs are 2.90, 2.75 and 2.70 eV) [102]. Since the π–π* transition involves a negative (electron) charge migration to the alkene part, it is more favorable for the stronger electron acceptor –(C=O)–S–CH_3 than for the weaker ones –(C=O)–O–CH_3 and –(C=O)–NH_2. Hence, the π–π* state is energetically lowered in the case of the S-substituent.

5.2. Heteroatom influence on twisted geometries

Given that the experimental studies of Refs. [8,49,50] indicate a strong heteroatom effect on the observed isomerisation dynamics, we examine here the changes occurring in the energetics of the twisted extrema ($S^{\alpha}_{1,min}$, $S^{\beta}_{1,min}$) identified in Section 4. Again, we are not able to provide a full picture of the heteroatom influence – which would involve, in particular, the influence on the reaction path barrier(s) – but we focus here upon the stationary geometries which have been examined in the previous section.

Among the three S_1 stationary points of the $pCTMe^-\cdot 2H_2O$ species (Section 4), the two twisted minima – i.e., the $S^{\alpha}_{1,min}$and $S^{\beta}_{1,min}$ stationary points that correspond to torsion around the C_4–C_7 single bond and C_7=C_8 double bond, respectively – exist for all heteroatom substitutions as well. They are energetically shifted, in a way that is further explained below, but the basic S_1 topology around these stationary points should remain unchanged. As for the planar $S_{1,TS}$ point (Section 4), this point was localized for the $pCMe^-\cdot 2H_2O$ and $pCTMe^-\cdot 2H_2O$ species, but it was not found for the nitrogen substituted species ($pCM^-\cdot 2H_2O$): That is, relaxation from the FC region leads directly to the twisted geometry $S^{\alpha}_{1,min}$ in the $pCM^-\cdot 2H_2O$ case. (However, we assume that the stationary point in fact does exist in the amide species as well.)

For all three chromophore species, the general pattern of geometry relaxation thus remains the same. That is, relaxation from the FC point initially involves alteration of the bond and valence angles, leading to an intermediate saddle point geometry ($S_{1,TS}$). From there, a barrierless process leads to the twisted minimum with respect to the single bond. The second minimum geometry, relating to a twist around the double bond, can only be accessed by surmounting a barrier [91].Given these similarities, the heteroatom effect mainly relates to a change of the energetics, as illustrated in Table 7 and Fig. 9. The following trends are observed:

(i) For the α-twisted geometry $S^{\alpha}_{1,min}$, the S_1–S_0 energy gap decreases in the order N ($\Delta_{S_1-S_0} = 1.89$ eV) versus O ($\Delta_{S_1-S_0} = 1.84$ eV) versus S ($\Delta_{S_1-S_0} = 1.62$ eV). This is in agreement with an increasing stabilization of S_1 as a function of the electron acceptor strength.

(ii) For the β-twisted geometry ($S^{\beta}_{1,min}$), the inverse trend is observed: i.e., the S_1–S_0 energy gap (below referred to as β energy gap) decreases in the order S ($\Delta_{S_1-S_0} = 0.42$ eV) versus O ($\Delta_{S_1-S_0} = 0.19$ eV) versus N ($\Delta_{S_1-S_0} = 0.07$ eV). A stabilization of S_1 occurs with *decreasing* electron acceptor strength. Note that the stabilization is more pronounced in the presence of hydrogen bonding. (In fact, in the absence of hydrogen bonding, the S_1–S_0 gap in $pCTMe^-$ lies at 0.84 eV—exactly the same as the value determined by Groenhof et al. [33].)

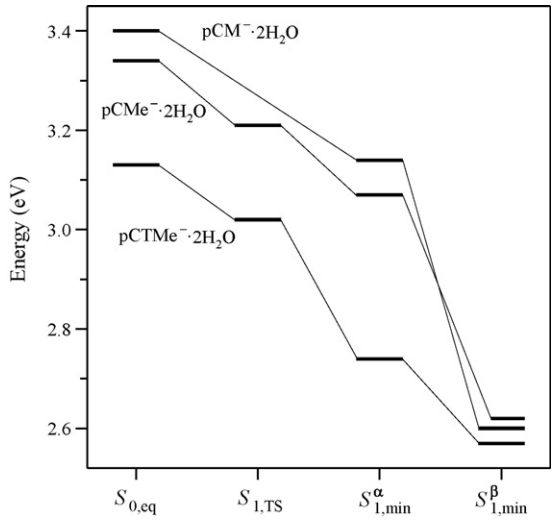

Fig. 9. Comparison of the $S_1(\pi–\pi^*)$ transition energies for $pCM^-·2H_2O$, $pCMe^-·2H_2O$ and $pCTMe^-·2H_2O$ at the different stationary points. For each chromophore, the respective ground state (CC2) energy at $S_{0,eq}$ is taken as the origin.

These observations are consistent with the opposite charge character of the two minima, as discussed in the preceding section. That is, the $S^{\beta}_{1,min}$ geometry favors electronic density to remain on the phenyl moiety (thus disfavoring strongly electron accepting heteroatoms). By contrast, at the $S^{\alpha}_{1,min}$ minimum geometry, a displacement of the electronic density towards the alkene moiety is favored.

The variation of the β energy gap as a function of the substituent (Table 7) implies that the distance between the $S^{\beta}_{1,min}$ minimum and the location of the S_1–S_0 conical intersection varies as a function of the substituent. This could have an important bearing upon the dynamical process: i.e., the conical intersection could become far easier accessible in the case of the N heteroatom than in the case of sulfur. This could be a possible reason for the differences observed in the solution-phase transient spectroscopy of the amide species as compared with the thio-ester: The amide exhibits photoisomerisation without formation of a spectroscopically observable intermediate, while the thio-ester is found to mainly relax to the initial *trans* form, *via* an intermediate that is spectroscopically observed [50]. The ester (i.e., oxygen-containing species) shows an intermediate behavior. However, the present study can provide only qualitative indications, in particular since the solvent influence can be substantial.

6. Influence of the environment

Due to the anionic nature of the chromophore and the marked charge transfer character of the S_1–S_0 transition, the influence of environmental effects is expected to be very pronounced. This concerns both electrostatic interactions with a polar/polarizable environment and hydrogen bonding interactions. In the native protein environment, an intricate interplay of various effects is observed, that can be selectively probed by comparing various mutants [24,40]. We have recently carried out an *ab initio* study that aims to unravel the effects of the individual amino acid residues on the PYP chromophore in its native protein environment [57]. In solution, the situation proves complex as well, involving both polarity and viscosity effects [8,19,46,48]. While the present paper does not focus on the influence of the environment, we summarize a number of observations for the $pCTMe^-·2H_2O$ and $pCTMe^-·2H_2O$[Arg52] species, along with certain conjectures put forward by Groenhof et al. [33] regarding the influence of the protein environment upon the electronic structure and dynamics.

As shown in our recent investigation of the PYP chromophore in its native protein environment [57], the excited-state electronic structure in the presence of the environment essentially retains the features described in this paper. In particular, the $S_1(\pi–\pi^*)$ state is quasi-isolated from the remaining manifold of excited electronic states. The chromophore in the native PYP environment should thus be considered as a specifically stabilized $pCTMe^-$ species. The same general observation holds true for the small complexes considered here.

6.1. Hydrogen bonding

An aspect that has already been discussed above (Section 3.4), and that is implicitly present in all of the calculations presented here, concerns the role of hydrogen bonding. The present study has in fact largely focussed on the hydrogen-bonded species $pCTMe^-·2H_2O$, whose ionization potential is significantly increased as compared with the bare chromophore. In the case of the native PYP chromophore, hydrogen bonding plays a similar role, but the dominant stabilization effect derives from the presence of the positively charged Arg52 residue that acts as a counter-ion [57].

Besides the effect of augmenting the ionization potential, the presence of hydrogen bonds has a marked effect on the energetics. This is clearly the case in the native protein, where hydrogen bonds to the Tyr42 and Glu46 amino acids provide the dominant energetic stabilization of the anionic species. As pointed out in Section 3.4, these energetic effects are mainly due to the chromophore's charge distribution: Hydrogen bonds tend to stabilize the states which exhibit a localized negative charge on the phenolate moiety. This is the case, in particular, for the S_0 ground state at the Franck-Condon geometry, and for the α-twisted minimum. By contrast, the S_0 state at the $S^{\beta}_{1,min}$ twisted minimum is *destabilized* since it exhibits an inverted charge distribution. At the same time, the S_1 state at the β-twisted minimum geometry is stabilized, leading to a decrease of the S_1–S_0 gap of approximately $\Delta_{S_1-S_0} = 0.4\,eV$ as compared with the "bare" chromophore (i.e., the gap for the bare chromophore is 0.8 eV while the gap for the $pCTMe^-·2H_2O$ species is $\Delta_{S_1-S_0} = 0.4\,eV$). The effect at the α-twisted minimum is opposite to this. These observations coincide with and explain the findings of Yamada et al. [27].

6.2. Role of the Arg52 residue

As mentioned above, the Arg52 residue plays the role of a counter-ion in the protein environment, and leads to a rise

of the ionization potential by several eV [57]. Besides its dramatic effect upon the ionization potential, the Arg residue is not found to play an important role as far as the energetics at the Franck-Condon geometry is concerned. This may appear surprising, since Coulombic interactions are expected to play an important role. However, as explained in further detail in Ref. [57], Coulombic effects act equally on the different states (at the Franck-Condon geometry)—hence, no net effect on the state separation appears. This is confirmed by various experimental investigations.

Despite these observations, the recent study by Groenhof et al. [33] suggests that the Arg52 residue has an extremely important energetic effect at the β-twisted geometry. As a result of the QM/MM calculations reported in Ref. [33], the S_1–S_0 energy gap at the β-twisted minimum decreases from $\Delta_{S_1-S_0} = 0.8$ eV (80 kJ/mol) to $\Delta_{S_1-S_0} = 0.01$ eV (1 kJ/mol) in the protein. A complementary calculation for the Arg52Gly mutant yields a 10-fold larger gap ($\Delta_{S_1-S_0} = 0.1$ eV, or 10 kJ/mol). The authors conclude that Arg52 plays a dominant role in stabilizing the $S^{\beta}_{1,\min}$ twisted structure.

While our calculations are in rather exact agreement with the value reported for the *in vacuo* energy gap of Ref. [33], $\Delta_{S_1-S_0} = 0.8$ eV, a calculation including the Arg52 residue yields a stabilization by only 0.3 eV, i.e., $\Delta_{S_1-S_0} = 0.5$ eV. The lack of agreement can be attributed to the fact that the position of the Arg52 residue might not be identical in the respective calculations. Notably, Ref. [33] asserts that the Arg52 residue is "located just above the negatively charged chromophore ring". By contrast, the geometry we refer to here corresponds to the X-ray data of Ref. [18] and implies that the Arg52 residue is located sideways with respect to the chromophore. The question of geometry effects thus remains to be clarified.

The study of Ref. [33] further suggests that the presence of the Arg52 residue leads to an important topology change, in that the α-twisted minimum would disappear while the β-twisted minimum would become directly accessible. However, as our preliminary calculations show, the twist around the C_4–C_7 bond in the presence of Arg52 still leads to a lowering of the $S_1(\pi$–$\pi^*)$ state, i.e. the $S^{\alpha}_{1,\min}$ minimum again exists. The conclusion of Ref. [33] is therefore not confirmed and further studies will be necessary to clarify this key aspect.

7. Conclusions

We have reported on high-level *ab initio* (CC2) calculations for selected geometries of the PYP *p*-coumaric thio-ester chromophore and various heteroatom substituent analogs. Particular emphasis was placed on the $S_1(\pi$–$\pi^*)$ state which plays a central role in the photochemistry of PYP. Even though the present study does not give a comprehensive picture of the S_1 state topology and the S_1–S_0 nonadiabatic coupling region, certain key aspects have been identified that will determine the isomerisation process. These aspects are briefly summarized here:

(i) The $S_1(\pi$–$\pi^*)$ state is essentially isolated from the other excited states of the anionic species; thus a two-state S_1–S_0 model for the isomerisation is appropriate. This is in contrast to the neutral chromophore, where the S_1 and S_2 states are close even at the Franck-Condon geometry [31,56]. As we have recently shown [57], the picture of an isolated S_1 state carries over to the chromophore in its native protein environment.

(ii) The anionic chromophore features a strong admixture of a quinone-like structure, such that the single bond adjacent to the phenol ring acquires some double-bond character, while the double bond conjugated with the ring acquires some single-bond character. In the S_0 ground state, the negative charge remains essentially localized on the phenolate moiety, while the S_1 state features a pronounced charge migration to the alkene part.

(iii) The chromophore features two torsional pathways leading to the respective minima $S^{\alpha}_{1,\min}$ and $S^{\beta}_{1,\min}$. That is, besides the conventional double-bond twist (β), a twist with respect to the single bond adjacent to the aromatic ring (α) becomes accessible. This can be interpreted as a consequence of the chromophore's quinone-like electronic structure features. The $S^{\alpha}_{1,\min}$ minimum is reached by a barrierless process from the FC geometry, but does not lead to an S_1–S_0 nonadiabatic decay since the S_1–S_0 gap remains substantial ($\Delta_{S_1-S_0} = 1.62$ eV). By contrast, the $S^{\beta}_{1,\min}$ minimum is located much closer to an S_1–S_0 intersection ($\Delta_{S_1-S_0} = 0.42$ eV); however, this minimum cannot be reached directly from the FC geometry.

(iv) The S_1 charge distribution exhibits substantial changes as a function of geometry. In particular, (i) a marked polarization effect, i.e., charge separation trend, is observed at the twisted minima, and (ii) an inversion of the electronic structure character is observed for the $S^{\beta}_{1,\min}$ minimum. We conjecture that this is due to the vicinity to a S_1–S_0 conical intersection. Certain features of the charge evolution can be accounted for by a two-electron two-orbital model (Section 4.2).

(v) The S_1–S_0 gap is a sensitive function of the heteroatoms (S, O, N). In particular, the N-substituted species features an energy gap at the $S^{\beta}_{1,\min}$ geometry that is as small as $\Delta_{S_1-S_0} = 0.07$ eV, as compared with 0.42 eV for the S-substituted chromophore (Section 5). This can have an important bearing on the dynamical process. As suggested by recent experiments in solution [8,49,50] the yield of the *cis* isomer is much higher in the case of the N-substituted species as compared with the O- and S-substituted chromophore analogs (in these latter cases, the *cis* form is essentially not observed). This could be a consequence of the fact that the S_1–S_0 conical intersection is significantly closer to the $S^{\beta}_{1,\min}$ minimum in the case of the amide species, thus facilitating the S_1–S_0 transition.

(vi) Likewise, the S_1–S_0 gap is a function of environmental effects (hydrogen bonds, local protein environment). Both hydrogen bonding and the presence of the Arg52 residue lead to a reduction by 0.3–0.4 eV of the S_1–S_0 gap at the $S^{\beta}_{1,\min}$ geometry. This is related to the stabilization/destabilization of the negative charge at the twisted

minima. A similar behavior was previously observed by Yamada et al. [27].

While some of the above-mentioned aspects have been addressed in previous work, notably by Groenhof et al. [33] and Yamada et al. [27], the present study clarifies certain previous findings. In particular, we have confirmed the observation in Ref. [33] that the $S^{\beta}_{1,min}$ minimum features the negative charge on the phenolate moiety, but have analyzed this finding in the context of the global geometry dependence of the S_1 charge distribution. While the $S_1(\pi–\pi^*)$ state is *a priori* characterized by a marked shift of the negative charge towards the alkene part, certain geometries – in particular the $S^{\beta}_{1,min}$ geometry – feature an inverted charge distribution pattern, with the charge localized on the phenolate moiety. We attribute this inversion to the vicinity of the S_1–S_0 conical intersection (Section 4).

Our detailed analysis of the charge distribution patterns is key to the understanding of both heteroatom effects and environmental effects (Sections 5 and 6). For example, an increasing heteroatom electron acceptor strength reduces the S_1–S_0 energy gap at the $S^{\alpha}_{1,min}$ geometry but increases the gap at the $S^{\beta}_{1,min}$ geometry. Likewise, hydrogen bonding destabilizes the $S^{\alpha}_{1,min}$ minimum but stabilizes the $S^{\beta}_{1,min}$ minimum. These observations provide the first steps in the systematic interpretation of the effects of the protein environment on the isomerisation process. They also pave the way to an understanding of static and dynamic solvent effects [50].

Many questions remain open, in particular regarding the conditions which would lead to a topology change of the S_1 potential, such that the $S^{\beta}_{1,min}$ minimum would become directly accessible. While the study of Ref. [33] suggests that the presence of the Arg52 residue leads to such a topology change, we have not been able to confirm this observation. (As explained above, this is possibly a consequence of the fact that different X-ray geometries have been referred to in this work, see Section 6.) In all systems we have considered, the simultaneous presence of the α- and β-twisted minima persists, along with the presence of a barrier on the β-twisted path. The presence of the α-twisted minimum could in fact account for the observation of long-lived S_1 intermediates, as reported by Zewail and collaborators for a ketone analog of the PYP chromophore in the gas phase [21]. In fact, the α-twisted structure is in principle observable, due to its non-negligible oscillator strengths. (According to results of the present study it is 0.06 a.u. as compared with $<10^{-3}$ a.u. for the $S^{\beta}_{1,min}$ minimum). However, the global effect of the protein environment could lead to a strong destabilization of the $S^{\alpha}_{1,min}$ minimum, along with a coincidence of the $S^{\beta}_{1,min}$ minimum with the conical intersection geometry, as suggested in Ref. [33]. We plan to investigate this question, using similar strategies as in our recent study of Ref. [57] which unravels the effects of the individual amino acids at the FC geometry. Another important objective in this context is the characterization of the barrier towards the double-bond twisted minimum ($S^{\beta}_{1,min}$).

Finally, we point out that certain similarities and differences exist as compared with the isomerisation processes in other polar double-bond systems. In particular, the charge translocation feature discussed above (i.e., a marked shift of the negative charge from the phenolate moiety to the alkene moiety in the S_1 state) bears some analogy to the translocation of a (positive) charge in retinal type systems. Thus, we believe that a two-electron two-orbital model is useful in the interpretation of the S_1–S_0 charge transfer (Section 4.2). On the other hand, the existence of the additional $S^{\alpha}_{1,min}$ minimum, i.e., the twisted geometry with respect to the formal single bond adjacent to the ring, is an important feature which is specific to systems which exhibit double bonds conjugated with an electron donor-acceptor substituted aromatic system. We suggest to further investigate the generic nature of isomerisation processes in such extended conjugated systems.

Acknowledgments

This work was supported in part by a CNRS/DFG collaboration project and by NSF grant CHE-0417570. We thank Monique Martin, Pascale Changenet-Barret, and Pascal Plaza for valuable discussions.

References

[1] W.W. Sprenger, W.D. Hoff, J.P. Armitage, K.J. Hellingwerf, J. Bacteriol. 175 (1993) 3096.
[2] U.K. Genick, S.M. Soltis, P. Kuhn, I.L. Canestrelli, E.D. Getzoff, Nature 392 (1998) 206.
[3] P. Kukura, D.W. McCamant, S. Yoon, D.B. Wandschneider, R.A. Mathies, Science 310 (2005) 1006.
[4] K.J. Hellingwerf, J. Hendriks, T. Gensch, J. Phys. Chem. A 107 (2003) 1082.
[5] M.A. Cusanovich, T.E. Meyer, Biochemistry 42 (2003) 4759.
[6] J.A. Kyndt, T.E. Meyer, M.A. Cusanovich, Photochem. Photobiol. Sci. 3 (2004) 519.
[7] N. Mataga, H. Chosrowjan, S. Taniguchi, J. Photochem. Photobiol. C: Photochem. Rev. 5 (2004) 155.
[8] P. Changenet-Barret, A. Espagne, P. Plaza, K.J. Hellingwerf, M.M. Martin, New J. Chem. 29 (2005) 527.
[9] D.S. Larsen, R. van Grondelle, ChemPhysChem 6 (2005) 828.
[10] A. Baltuska, I. Stokkum, A. Kroon, R. Monshouwer, K.J. Hellingwerf, R. van Grondelle, Chem. Phys. Lett. 270 (1997) 263.
[11] H. Chosrowjan, N. Mataga, N. Nakashima, Y. Imamoto, F. Tokunaga, Chem. Phys. Lett. 270 (1997) 267.
[12] H. Chosrowjan, N. Mataga, Y. Shibata, Y. Imamoto, F. Tokunaga, J. Phys. Chem. B 102 (1998) 7695.
[13] S. Devanathan, A. Pacheco, L. Ujj, M. Cusanovich, G. Tollin, S. Lin, N. Woodbury, Biophys. J. 77 (1999) 1017.
[14] T. Masciangioli, S. Devanathan, M.A. Cusanovich, G. Tollin, M.A. El-Sayed, Photochem. Photobiol. 72 (2000) 639.
[15] Y. Imamoto, M. Kataoka, F. Tokunaga, T. Asahi, H. Masuhara, Biochemistry 40 (2001) 6047.
[16] Y. Imamoto, M. Kataoka, R. Liu, Photochem. Photobiol. 76 (2002) 584.
[17] M.L. Groot, L. Wilderen, D.S. Larsen, M. Horst, I. Stokkum, K.J. Hellingwerf, R. van Grondelle, Biochemistry 42 (2003) 10054.
[18] R. Kort, K.J. Hellingwerf, R.B.G. Ravelli, J. Biol. Chem. 279 (2004) 26417.
[19] P. Changenet-Barret, A. Espagne, S. Charier, J.-B. Baudin, L. Jullien, P. Plaza, K.J. Hellingwerf, M.M. Martin, Photochem. Photobiol. Sci. 3 (2004) 823.
[20] H. El-Gezawy, W. Rettig, A. Danel, G. Jonusauskas, J. Phys. Chem. B 109 (2005) 18699.

[21] I. Lee, W. Lee, A.H. Zewail, Proc. Natl. Acad. Sci. U.S.A. 103 (2006) 258.
[22] K. Heyne, O.F. Mohammed, A. Usman, J. Dreyer, E. Nibbering, M.A. Cusanovich, J. Am. Chem. Soc. 127 (2005) 18100.
[23] L. Wilderen, M. Horst, I. Stokkum, K.J. Hellingwerf, R. van Grondelle, M.L. Groot, Proc. Natl. Acad. Sci. U.S.A. 103 (2006) 15050.
[24] P. Changenet-Barret, P. Plaza, M.M. Martin, H. Chosrowjan, S. Taniguchi, N. Mataga, Y. Imamoto, M. Kataoka, Chem. Phys. Lett. 434 (2007) 320.
[25] T. Yamato, N. Niimura, N. Go, Proteins 32 (1998) 268.
[26] V. Molina, M. Merchán, Proc. Natl. Acad. Sci. U.S.A. 98 (2001) 4299.
[27] A. Yamada, S. Yamamoto, T. Yamato, T. Kakitani, J. Mol. Struct. (Theochem.) 536 (2001) 195.
[28] G. Groenhof, M.F. Lensink, H.J.C. Berendsen, J.G. Snijders, A.E. Mark, Proteins 48 (2002) 202.
[29] G. Groenhof, M.F. Lensink, H.J.C. Berendsen, A.E. Mark, Proteins 48 (2002) 212.
[30] I. Antes, W. Thiel, W.F.Eu. van Gunsteren, Biophys. J. 31 (2002) 504.
[31] C. Ko, B. Levine, A. Toniolo, L. Manohar, S. Olsen, H.-J. Werner, T.J. Martínez, J. Am. Chem. Soc. 125 (2003) 12710.
[32] M.J. Thompson, D. Bashford, L. Noodleman, E.D. Getzoff, J. Am. Chem. Soc. 125 (2003) 8186.
[33] G. Groenhof, M. Bouxin-Cademartory, B. Hess, S.P. de Visser, H.J.C. Berendsen, M. Olivucci, A.E. Mark, M.A. Robb, J. Am. Chem. Soc. 126 (2004) 4228.
[34] A. Yamada, T. Ishikura, T. Yamato, Proteins 55 (2004) 1063.
[35] A. Yamada, T. Ishikura, T. Yamato, Proteins 55 (2004) 1070.
[36] K. Mihara, O. Hisatomi, Y. Imamoto, M. Kataoka, F. Tokunaga, J. Biochem. 121 (1997) 876.
[37] U.K. Genick, S. Devanathan, T.E. Meyer, I.L. Canestrelli, E. Williams, M.A. Cusanovich, G. Tollin, E.D. Getzoff, Biochemistry 36 (1997) 8.
[38] R. Brudler, T.E. Meyer, U.K. Genick, S. Devanathan, T.T. Woo, D.P. Millar, K. Gerwert, M.A. Cusanovich, G. Tollin, E.D. Getzoff, Biochemistry 39 (2000) 13478.
[39] N. Mataga, H. Chosrowjan, Y. Shibata, Y. Imamoto, F. Tokunaga, J. Phys. Chem. B 104 (2000) 5191.
[40] N. Mataga, H. Chosrowjan, S. Taniguchi, N. Hamada, F. Tokunaga, Y. Imamoto, M. Kataoka, Phys. Chem. Chem. Phys. 5 (2003) 2454.
[41] M. Vengris, M. Horst, G. Zgrablić, I. Stokkum, S. Haacke, M. Chergui, K.J. Hellingwerf, R. Grondelle, D.S. Larsen, Biophys. J. 87 (2004) 1848.
[42] A.R. Kroon, W.D. Hoff, H.P.M. Fennema, J. Gijzen, G.-J. Koomen, J.W. Verhoeven, W. Crielaard, K.J. Hellingwerf, J. Biol. Chem. 271 (1996) 31949.
[43] P. Changenet-Barret, P. Plaza, M.M. Martin, Chem. Phys. Lett. 336 (2001) 439.
[44] D.L. Larsen, M. Vengris, I. Stokkum, M.A. van der Horst, R.A. Cordfunke, K.J. Hellingwerf, R. Grondelle, Chem. Phys. Lett. 369 (2003) 563.
[45] D.S. Larsen, M. Vengris, I. Stokkum, M.A. van der Horst, F. Weerd, K.J. Hellingwerf, R. Grondelle, Biophys. J. 86 (2004) 2538.
[46] A. Espagne, P. Changenet-Barret, S. Charier, J.-B. Baudin, L. Jullien, P. Plaza, M.M. Martin, in: M.M. Martin, J.T. Hynes (Eds.), Femtochemistry and Femtobiology, Elsevier, 2004.
[47] M. Vengris, D.S. Larsen, M. Horst, O. Larsen, K.J. Hellingwerf, R. Grondelle, J. Phys. Chem. B 109 (2004) 4197.
[48] A. Espagne, D.H. Paik, P. Changenet-Barret, M.M. Martin, A.H. Zewail, ChemPhysChem 7 (2006) 1717.
[49] A. Espagne, P. Changenet-Barret, P. Plaza, M.M. Martin, J. Phys. Chem. A 110 (2006) 3393.
[50] A. Espagne, P. Changenet-Barret, J. Baudin, P. Plaza, M.M. Martin, J. Photochem. Photobiol. A 185 (2007) 242.
[51] A. Usman, H. Masuhara, T. Asahi, J. Phys. Chem. B 110 (2006) 20085.
[52] W.L. Ryan, D.J. Gordon, D.H. Levy, J. Am. Chem. Soc. 124 (2002) 6194.
[53] I.B. Nielsen, S. Boyé-Péronne, M.O.A. El Ghazaly, M.B. Kristensen, S. Brøndsted Nielsen, L.H. Andersen, Biophys. J. 89 (2005) 2597.
[54] M. de Groot, W.J. Buma, J. Phys. Chem. A 109 (2005) 6135.
[55] M. de Groot, W.J. Buma, E.V. Gromov, I. Burghardt, H. Köppel, L.S. Cederbaum, J. Chem. Phys. 125 (2006) 204303.
[56] E.V. Gromov, I. Burghardt, H. Köppel, L.S. Cederbaum, J. Phys. Chem. A 109 (2005) 4623.
[57] E.V. Gromov, I. Burghardt, H. Köppel, L.S. Cederbaum, J. Am. Chem. Soc. 129 (2007) 6798.
[58] O. Christiansen, H. Koch, P. Jørgensen, Chem. Phys. Lett. 243 (1995) 409.
[59] A. Xie, W.D. Hoff, A.R. Kroon, K. Hellingwerf, J. Biochem. 35 (1996) 14671.
[60] H. Sekino, R. Bartlett, J. Int. J. Quant. Chem., Quant. Chem. Symp. 18 (1984) 255.
[61] J. Geertsen, M. Rittby, R. Bartlett, J. Chem. Phys. Lett. 164 (1989) 57.
[62] J.F. Stanton, R.J. Bartlett, J. Chem. Phys. 98 (1993) 7029.
[63] A.B. Trofimov, G. Stelter, J. Schirmer, J. Chem. Phys. 117 (2002) 6402.
[64] E.V. Gromov, A.B. Trofimov, N.M. Vitkovskaya, J. Schirmer, H. Köppel, J. Chem. Phys. 119 (2003) 737.
[65] F. Weigend, M. Häser, H. Patzelt, R. Ahlrichs, Chem. Phys. Lett. 294 (1998) 143.
[66] R. Ahlrichs, Phys. Chem. Chem. Phys. 6 (2004) 5119.
[67] R. Ahlrichs, M. Bär, M. Häser, H. Horn, C. Kölmel, Chem. Phys. Lett. 162 (1989) 165.
[68] J.F. Stanton, J. Gauss, J.D. Watts, P.G. Szalay, R.J. Bartlett, ACES II The Mainz–Austin–Budapest version, with contributions from A.A. Auer, D.B. Bernholdt, O. Christiansen, M.E. Harding, M. Heckert, O. Heun, C. Huber, D. Jonsson, J. Jusélius, W.J. Lauderdale, T. Metzroth, C. Michauk, K. Ruud, F. Schiffmann, A. Tajti, Integral packages included are VMOL (J. Almlöf, P.R. Taylor); VPROPS (P. Taylor) ABACUS; (T. Helgaker, H.J. Aa. Jensen, P. Jørgensen, J. Olsen, P.R. Taylor).
[69] T.H. Dunning Jr., J. Chem. Phys. 90 (1989) 1007.
[70] W. von Niessen, J. Schirmer, L.S. Cederbaum, Comput. Phys. Rep. 1 (1984) 57.
[71] R.A. Kendall, T.H. Dunning Jr., R.J. Harrison, J. Chem. Phys. 96 (1992) 6796.
[72] M.J. Frisch, et al., Gaussian 03 Revision C.02, Gaussian, Inc., Wallingford, CT, 2004.
[73] D. Rappoport, F. Furche, Lect. Notes Phys. 706 (2006) 337.
[74] A. Dreuw, M. Head-Gordon, J. Am. Chem. Soc. 126 (2004) 4007.
[75] M. de Groot et al., unpublished results.
[76] W.D. Hoff, B. Devreese, R. Fokkens, I.N. Nugteren-Roodzant, J. Van Beeumen, N. Nibbering, K. Hellingwerf, J. Biochem. 35 (1996) 1274.
[77] M. Yoda, H. Houjou, Y. Inoue, M. Sakurai, J. Phys. Chem. B 105 (2001) 9887.
[78] A. Xie, L. Kelemen, J. Hendriks, B.J. White, K.J. Hellingwerf, W.D. Hoff, Biochemistry 40 (2001) 1510.
[79] L.L. Premvardhan, M.A. van der Horst, K.J. Hellingwerf, R. van Grondelle, Biophysics 84 (2003) 3226.
[80] The two π–π^* states can in fact be considered as "perturbed" L_a and L_b states of benzene.
[81] Note that in our previous work [56] the ordering of the two π–π^* states is reversed, as a consequence of the strong configurational mixing even for small changes in the molecular structure. Furthermore, the methyl ester was replaced by a hydroxy group in this study.
[82] In this case the assignment to the π–π_1^* and π–π_2^* states is arbitrary.
[83] The autoionization-induced linewidth has not been precisely determined as yet [53].
[84] The same holds true for the n–π_1^* state, see discussion in Ref. [56].
[85] The n_{ph}–π_1^* state was found to become higher in energy due to the effect of hydrogen bonding [57].
[86] S. Feuerbacher, T. Sommerfeld, L.S. Cederbaum, J. Chem. Phys. 120 (2004) 3201.
[87] Note, that there are two equivalent $S^{\alpha}_{1,\min}$ minima resulting from the clockwise or counterclockwise rotation of the alkene fragment around the single bond.
[88] According to Groenhof et al. [33], the single-bond twisted minimum disappears when the chromophore's local environment is taken into account; at the same time, the barrier for reaching the double-bond twisted minimum is diminished or disappears entirely.
[89] J. Michl, V. Bonačić-Koutecký, Electronic Aspects of Organic Photochemistry, J. Wiley & Sons, Inc., New York, 1990.

[90] Similarly to the case of the α-twist, two equivalent $S^{\beta}_{1,min}$ minima exist which result from the clockwise or counterclockwise rotation of the carbonyl fragment around the double bond.
[91] In the present study we have not optimized the transition state(s) (barrier(s)) towards the double-bond twisted configuration ($S^{\beta}_{1,min}$). This would involve identifying the reaction coordinate, minimum energy path and topological features of the S_1 PES which is beyond the scope of the present study. These issues will be addressed in forthcoming investigations.
[92] F. Momicchioli, A.S. Tatikolov, D. Vanossi, G. Ponterini, Photochem. Photobiol. Sci. 3 (2004) 396.
[93] M. Dekhtyar, W. Rettig, J. Phys. Chem. A 111 (2007) 2035.
[94] V. Bonačić-Koutecký, J. Koutecký, J. Michl, Angew. Chem. 26 (1987) 170.
[95] V. Bonačić-Koutecký, K. Schöffel, J. Michl, J. Theor. Chem. Acc. 72 (1987) 459.
[96] Z.R. Grabowski, K. Rotkiewicz, W. Rettig, Chem. Rev. 103 (2003) 3899.
[97] M. Garavelli, T. Vreven, P. Celani, F. Bernardi, M.A. Robb, M. Olivucci, J. Am. Chem. Soc. 120 (1998) 1285.
[98] F. Molnar, M. Ben-Nun, T.J. Martínez, K. Schulten, THEOCHEM 506 (2000) 169.
[99] I. Burghardt, L.S. Cederbaum, J.T. Hynes, Faraday Discuss. Chem. Soc. 127 (2004) 395.
[100] I. Burghardt, J.T. Hynes, J. Phys. Chem. A 110 (2006) 11411.
[101] B. Borucki, H. Otto, T.E. Meyer, M.A. Cusanovich, M.P. Heyn, J. Phys. Chem. B 109 (2005) 629.
[102] Here we imply that the acceptor properties (with regard to the electron involved in the π–π^* excitation) can be estimated from the electron affinity (EA) of the neutral species or the first ionization potential (IP) of the anion. Within the same geometry, calculational method and basis set, the EA of the neutral and IP of the anion should be equal.